AD-A057 686 NAVAL RESEARCH LAB WASHINGTON D C F/G 20/5
THEORY OF ELECTRON CYCLOTRON MASER INTERACTIONS IN A CAVITY AT --ETC(U)
APR 78 K R CHU

UNCLASSIFIED NRL-MR-3672 SBIE-AD-E000 181 NL

| OF |
AD
A057686

END
DATE
FILMED
9-78
DDC

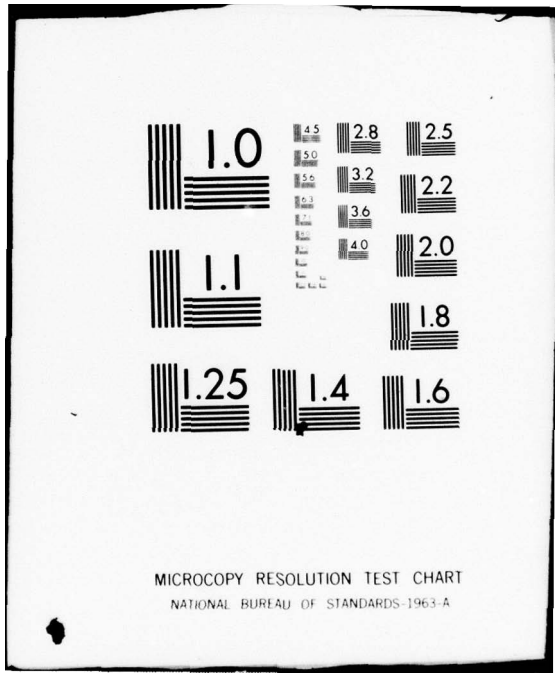
1.0
1.1
1.25
1.4
1.6
1.8
2.0
2.2
2.5
2.8
3.2
3.6
4.0
4.5
5.0
5.6
6.3
MICROCOPY RESOLUTION TEST CHART
NATIONAL BUREAU OF STANDARDS-1963-A

(12)
5C

NRL Memorandum Report 3672

# Theory of Electron Cyclotron Maser Interactions In A Cavity At The Harmonic Frequencies

K. R. Chu

*Plasma Physics Division*

LEVEL II

April 1978



NAVAL RESEARCH LABORATORY
Washington, D.C.

SECURITY CLASSIFICATION OF THIS PAGE (When Data Entered)

## REPORT DOCUMENTATION PAGE

READ INSTRUCTIONS BEFORE COMPLETING FORM

1. REPORT NUMBER: NRL Report 3672
2. GOVT ACCESSION NO.:
3. RECIPIENT'S CATALOG NUMBER:

4. TITLE (and Subtitle): THEORY OF ELECTRON CYCLOTRON MASER INTERACTIONS IN A CAVITY AT THE HARMONIC FREQUENCIES
5. TYPE OF REPORT & PERIOD COVERED: Interim report on a continuing NRL Problem
6. PERFORMING ORG. REPORT NUMBER:

7. AUTHOR(s): K. R. Chu
8. CONTRACT OR GRANT NUMBER(s):

9. PERFORMING ORGANIZATION NAME AND ADDRESS: Naval Research Laboratory, Washington, D. C. 20375
10. PROGRAM ELEMENT, PROJECT, TASK AREA & WORK UNIT NUMBERS: NRL Prob. 77RO8-92 & 77RO8-95; Proj. No. XF54581091 & 8X363304D215

11. CONTROLLING OFFICE NAME AND ADDRESS: (1) Naval Electronic Systems Command, Wash. D. C.; (2) Ballistic Missile Defense Advanced Technology Center, Huntsville, ALA
12. REPORT DATE: April 1978
13. NUMBER OF PAGES: 38

14. MONITORING AGENCY NAME & ADDRESS (if different from Controlling Office): 38p.
15. SECURITY CLASS. (of this report): UNCLASSIFIED
15a. DECLASSIFICATION/DOWNGRADING SCHEDULE:

16. DISTRIBUTION STATEMENT (of this Report)

Approved for public release; distribution unlimited.

NRL-MR-3672

17. DISTRIBUTION STATEMENT (of the abstract entered in Block 20, if different from Report)

SBIE AD-E000 181

18. SUPPLEMENTARY NOTES

19. KEY WORDS (Continue on reverse side if necessary and identify by block number)

electron cyclotron maser
harmonic frequencies
parameter optimization
Larmor radius

20. ABSTRACT (Continue on reverse side if necessary and identify by block number)

A theory of the cyclotron maser interactions between an annular electron beam and the standing electromagnetic wave in a cavity structure is formulated on the basis of the relativistic Vlasov equation and the Maxwell equations. Detailed analytical expressions for the beam-wave coupling coefficient, beam energy gain, and threshold beam power have been derived for the fundamental and higher cyclotron harmonics. Physical interpretations of these results and comparison with cyclotron maser interactions in a waveguide structure will be presented. Methods of parameter optimization and their applications to experiments will be illustrated through numerical examples.

DD FORM 1 JAN 73 1473 EDITION OF 1 NOV 65 IS OBSOLETE
S/N 0102-LF-014-6601

SECURITY CLASSIFICATION OF THIS PAGE (When Data Entered)

## CONTENTS


I. INTRODUCTION ..... 1

II. MODEL AND FORMULATION ..... 5

III. DISTRIBUTION FUNCTION FOR A MAGNETRON TYPE ELECTRON BEAM ..... 8

IV. RESULT ..... 11

V. DISCUSSION ..... 22

REFERENCES ..... 24

APPENDIX A – EVALUATING THE INTEGRAL SERIES $I_s(a_0,a_L)$ ..... 28

# THEORY OF ELECTRON CYCLOTRON MASER INTERACTIONS IN A CAVITY AT THE FUNDAMENTAL AND HIGHER CYCLOTRON HARMONICS

## I. INTRODUCTION

In recent years, there has been increasing interest in an electromagnetic radiation mechanism known as the electron cyclotron maser.[1-3] In addition to its fundamental importance as a new scientific phenomenon, it has been the basis for a new type of microwave devices[4,5] (gyrotrons) capable of generating microwave at unprecedented power levels in the centimeter through submillimeter wavelength regime. This new source of high power microwaves has shown great promises for plasma heating[6] in fusion devices and opened new areas of radar applications. The cyclotron maser radiation mechanism originates from a relativistic effect. For the simplicity of illustration, we consider an ensemble of monoenergetic electrons in the presence of a uniform magnetic field $B_0$ and assume that the electrons have no velcoity along the magnetic field, hence they all gyrate with the same Larmor radius. Initially, the phases of electrons in their cyclotron orbits are random, so no radiation will be emitted. But phase bunching can occur because of the dependence of the electron cyclotron frequency on the relativistic electron mass. Those electrons that are decelerated in the wave electric field become lighter, rotate faster, and hence accumulate phase lead while those electrons that are accelerated rotate slower and accumulate phase lag. This will result in phase bunching such that the electrons radiate coherently at the frequency

$$\omega \simeq s\Omega_e/\gamma \tag{1}$$

Manuscript submitted November 28, 1977.

where $\Omega_e = eB_0/mc$, $\gamma$ is the relativistic factor, and $s$ is an integer. Original investigations of the physical processes were carried out in the late 1950's by Twiss,[1] Schneider,[2] and Gaponov,[3] and early experimental observations were made by Hirshfield and Wachtel,[7] and Chou and Pantell.[8] Further theoretical[9-28] and experimental[29-42] studies as well as review works[4,5] have appeared frequently in literature. The azimuthal bunching mechanism described here and the well known Lorentz force induced axial bunching mechanism are evidently of different physical origins; however, as shown in a recent comparative study,[15] the two mechanisms always combine in such a way as to *offset* one another. The azimuthal bunching mechanism dominates for waves with phase velocity greater than the speed of light and vice versa, hence the cyclotron maser radiation can be generated only in a fast wave structure.

Theoretical cyclotron maser studies have generally been based on two models, each corresponding to a common experimental configuration. In the first model,[9-16] the electromagentic wave grows as an instability due to the velocity space anisotropy of the electron medium. It applies to travelling wave amplification in waveguide structures. In the second model,[17-28] on which the present analysis will be based, the electron beam interacts with the constant amplitude standing wave of a cavity structure. It applies to beam sustained oscillations in a finite $Q$ cavity.

In previous analytical studies[17,18,21-24,27] of the second model, it has been generally assumed that the electron Larmor radius is small compared with the radial scale length of the field structure so that field variations in the radial direction can be neglected. This assumption simplifies the analysis considerably while still leading to accurate results for the fundamental cyclotron harmonic interaction. However, information concerning higher cyclotron harmonic interactions has been precluded under this assumption because the higher harmonic interaction is essentially a finite Larmor radius effect. A unique advantage of the cyclotron maser comes from its capability to generate high power submillimeter waves. Using the relation

$\omega \simeq s\Omega_e/\gamma$ [Eq. (1)], we find that generation of submillimeter waves through the fundamental cyclotron harmonic ($s = 1$) requires an external magnetic field in excess of 100 kG, apparently too high to be practical. Thus interactions at high cyclotron harmonics become especially advantageous if large magnetic field is to be avoided. In view of these considerations, our emphasis in the present study will be on the higher cyclotron harmonic interactions.

Starting from the relativistic Vlasov equation and the Maxwell equations, we calculate the linear responses of an annular electron beam as it passes through the constant amplitude fields of a cavity structure. In contrast to previous treatments, the exact spatial field variations (radial variation in particular) have been incorporated and the electron Larmor radius has been kept arbitary. From the linear beam responses, the beam-wave coupling coefficient and the beam energy gain function are derived for harmonic interactions. On the basis of these results, conditions for maximum beam-wave coupling with respect to such parameter as beam position, beam energy, and cavity length can be found. It is shown that, for each mode of operation, there exists a threshold beam power below which the cavity oscillations can not be started. In general, the higher the cyclotron harmonic, the higher the thresold beam power, and the longer the cavity, the lower the threshold beam power. It is found that such threshold conditions can become very restrictive for higher cyclotron harmonics, hence in such operations it is desirable to have parameter fully optimized so as to lower the threshold conditions. In this regard, the analyses to be presented could be of considerable importance in assessing the feasibility of experimental goals and in selecting the proper modes and parameters to achieve them.

In Section I, the problem is formulated for a general beam distribution function. In Section II, we specialize to a distribution function consistent with the beam generated in a magnetron-type electron gun commonly used for cyclotron maser experiments. In Section III, the final results are presented, together with physical interpretations and numerical examples. A comparison is made between the nature of cyclotron maser interactions in a cavity structure

and that in a waveguide structure. A numerical code has been developed as an independent check of the analytical results. Section IV discusses the validity of the approximations used and some nonlinear aspects of the problem.

## II. MODEL AND FORMULATION

Figures 1a and b show the configuration of the electron cyclotron maser system under study. It consists of an annular electron beam propagating inside a circular cross-section cavity (radius $r_w$, length L). The axis of the electron beam coincides with that of the cavity. The electrons, guided by an applied uniform magnetic field ($B_0 \mathbf{e}_z$), move along helical trajectories. The electrons have a substantial part of their kinetic energy in the form of transverse gyromotion and the rest in the form of axial motion. Two types of electron orbits are implicit in this model. The more common type is shown in Fig. 1a where the electron orbit does not encircle the axis. The other type has the electron orbit encircling the axis.

*The following simplifying assumptions are made:*

1. The electron beam distribution function and the cavity fields are both independent of the azimuthal angle $\theta$.

2. The beam is sufficiently tenuous so that its self electrostatic and magnetic fields are negligible compared with the cavity fields.

3. The cavity fields are of first order compared with the applied magnetic field $B_0$; and

4. The perturbed distribution function $f^{(1)}$ is of first order compared with the initial distribution function $f_0$.

For cyclotron maser interactions, it is well known[4] that the beam couples much more strongly with the TE mode than the TM mode. This together with assumption 1 will thus restrict our consideration to the $TE_{0nl}$ cavity mode, where $n$ and $l$ are the radial and axial eigenmode numbers, respectively. The field components of the $TE_{0nl}$ cavity mode are

$$E_\theta^{(1)} = E_{\theta 0}\, J_1 (k_n r) \sin k_z z \cos \omega t, \tag{2}$$

$$B_r^{(1)} = (k_z c/\omega)\, E_{\theta 0}\, J_1 (k_n r) \cos k_z z \sin \omega t, \tag{3}$$

and

$$B_z^{(1)} = -(k_n c/\omega)\, E_{\theta 0}\, J_0 (k_n r) \sin k_z z \sin \omega t, \tag{4}$$

where $k_z = \pi l/L$, $k_n = x_n/r_w$, $x_n$ is the $n$-th nonvanishing root of $J_1(x) = 0$, $\omega = (k_z^2 + k_n^2)^{1/2} c$ is the wave frequency, and superscript "(1)" indicates first order quantities.

The dynamics of the electron beam are described by the realtivistic Vlasov equation,

$$\frac{\partial f}{\partial t} + \mathbf{v} \cdot \frac{\partial f}{\partial \mathbf{r}} - e\left(\mathbf{E} + \frac{1}{c}\, \mathbf{v} \times \mathbf{B}\right) \cdot \frac{\partial f}{\partial \mathbf{p}} = 0. \tag{5}$$

Linearizing Eq. (5) by the use of the ordering schemes of assumptions 3 and 4, and integrating the resulting equation by the method of characteristics, we obtain

$$f^{(1)}(\mathbf{p}, \mathbf{r}, t) = \int_{t - z/v_z}^{t} dt'\, e\left[\mathbf{E}^{(1)}(\mathbf{r}', t') + \frac{1}{c}\, \mathbf{v}' \times \mathbf{B}^{(1)}(\mathbf{r}', t')\right] \cdot \frac{\partial}{\partial \mathbf{p}'} f_0 (\mathbf{r}', \mathbf{p}'), \tag{6}$$

where $\mathbf{v} = \mathbf{p}/\gamma m$, $\gamma = [1 + (p_\perp^2 + p_z^2)/m^2 c^2]^{1/2}$, the primed quantities are treated as functions of $t'$, and $\mathbf{r}$, $\mathbf{p}$ are, respectively, the values of $\mathbf{r}'$, $\mathbf{p}'$ at $t' = t$. The integration over $t'$ is to be carried out along the unperturbed (helical) orbits of the electrons. Along its orbit, an electron feels the axial as well as the radial variations of the electromagnetic fields, $\mathbf{E}^{(1)}$ and $\mathbf{B}^{(1)}$, given by Eqs. (2) through (4). An electron located at the axial position $z$ at time $t$ enters the cavity at time $t - z/v_z$. This determines the limits of the $t'$-integration in Eq. (6).

Methods for evaluating the integral in Eq. (6) are standard[43] and, for the present problem, involve the use of the following Bessel function identity[44]:

$$e^{is\theta_1} J_s (x_1) = \sum_{s' = -\infty}^{\infty} J_{s+s'} (x_2)\, J_{s'} (x_3)\, e^{is'\theta_2}, \tag{7}$$

where $x_1$, $x_2$, $x_3$, $\theta_1$ and $\theta_2$ are related through the triangle shown in Fig. 2 The lengthy algebra will not be detailed here. Instead, in Sec. IV, we will present detailed physical interpretations and an independent numerical check of the final results.

The perturbed distribution function $f^{(1)}$ as solved from Eq. (6) assumes the following form,

$$f^{(1)} = f_+^{(1)} + f_-^{(1)} \tag{8}$$

where

$$f_+^{(1)} = Im\left\{\frac{k_z c e E_{\theta 0}}{2\omega} e^{ik_z z - i\omega t}\left[\left(\frac{\omega}{k_z c} - \frac{p_z}{\gamma mc}\right)\frac{\partial f_0}{\partial p_{\perp -}} + \frac{p_{\perp}}{\gamma mc}\frac{\partial f_0}{\partial p_z}\right]\right.$$
$$\left.\cdot \sum_{s=-\infty}^{\infty} \sum_{s'=-\infty}^{\infty} i^{s'-1} \frac{J_s'(k_n r)\, G_{ss'}(k_n r_L) X \exp\left[-is'(\phi - \theta)\right]}{\omega - k_z v_z - s\Omega_e/\gamma}\right\}, \tag{9}$$

and $f_-^{(1)}$ is given by Eq. (9) with $\omega$ replaced by $-\omega$. In Eq. (9), $Im\{Z\}$ indicates the imaginary part of $Z$, $G_{ss'}(x) \equiv J_{s+s'}(x) dJ_s(x)/dx$, $\Omega_e \equiv eB_0/mc$, $r_L \equiv p_{\perp}/m\Omega_e$, $\phi$ and $\theta$ are respectively, the polar angles of the momentum and position vectors ( see Fig. 3), and $X \equiv 1 - \exp\left[i(\omega - k_z v_z - s\Omega_e/\gamma) z/v_z\right]$. The perturbed azimuthal current, $J_\theta^{(1)}$, can be written in terms of $f^{(1)}$ as

$$J_\theta^{(1)} = -e \int f^{(1)} v_\theta d^3p = -e \int_0^{\infty} p_{\perp} dp_{\perp} \int_{-\infty}^{\infty} dp_z \int_0^{2\pi} d\hat{\phi}\, f^{(1)} v_{\perp} \sin \hat{\phi}, \tag{10}$$

where $\hat{\phi} \equiv \phi - \theta$.

Inserting Eq. (8) into Eq. (10) and carrying out integrations by parts over $p_{\perp}$ and $p_z$, we obtain

$$J_\theta^{(1)} = J_{\theta +}^{(1)} + J_{\theta -}^{(1)}, \tag{11}$$

where

$$J_{\theta+}^{(1)} = Im\left\{\frac{e^2 E_{\theta 0}}{4m\omega}\, e^{i(k_z z - i\omega t)} \sum_{s=-\infty}^{\infty} \sum_{s'=-\infty}^{\infty} J_{s'}(k_n r)\right.$$

$$\cdot \int_0^{\infty} p_\perp dp_\perp \int_{-\infty}^{\infty} dp_z \int_0^{2\pi} d\hat{\phi}\, f_0\, i^{s'}\left[e^{-i(s'-1)\hat{\phi}} - e^{-i(s+1)\hat{\phi}}\right]$$

$$\cdot \left\{G_{ss'}(k_n r_L) p_\perp^2 [(\omega^2 - k_z^2 c^2) X/\gamma m^2 c^2 + iz\epsilon(1 - X)\right.$$

$$\cdot (\omega^2 - k_z^2 c^2 - k_z c^2 \epsilon / v_z) / mc^2 p_z] \gamma^{-2} \epsilon^{-2}$$

$$\left.\left. - (\omega - k_z p_z/\gamma m) X [2G_{ss'}(k_n r_L) + k_n r_L\, G'_{ss'}(k_n r_L)] \gamma^{-1} \epsilon^{-1} \right\}\right\}, \tag{12}$$

$$\epsilon \equiv \omega - k_z p_z/\gamma m - s\Omega_e/\gamma,$$

$$G'_{ss'}(x) = dG_{ss'}(x)/dx,$$

and $J_{\theta-}^{(1)}$ is given by Eq. (12) with $\omega$ replaced by $-\omega$.

The time averaged power gain (P) of all the electrons in the cavity is then

$$P = \omega \int_0^{\frac{2\pi}{\omega}} dt \int_0^{r_w} r dr \int_0^{L} dz\, J_\theta^{(1)}\, E_\theta^{(1)}. \tag{13}$$

Equation (13) is a general expression for the beam power gain. In the following section, we specialize to a particular distribution function which is considered to be most ideal for cyclotron maser operations.

## III. DISTRIBUTION FUNCTION FOR A MAGNETRON TYPE ELECTRON BEAM

Before Eq. (13) can be evaluated, a proper distribution function for the electron beam has to be constructed from the constants of motion of the system: $p_\perp, p_z$, and $P_\theta$, where

$$P_\theta = \gamma m r p_\perp \sin\hat{\phi} - \frac{1}{2}\frac{e}{c} B_0 r^2. \tag{14}$$

We are interested in a distribution function in which the electrons have arbitrary spread in $p_\perp$ and $p_z$, with their guiding centers uniformly distributed on a cyclinder of radius $r_0$ (see Fig. 1a). Such a distribution function is represented by

$$f_0 = K\,\delta\,(r_L^2 - 2cP_\theta/eB_0 - r_0^2)\; g\;(p_\perp, p_z), \tag{15}$$

where $\delta(x)$ is the Dirac delta function, $g(p_\perp, p_z)$ is an arbitrary function of $p_\perp$ and $p_z$ (to be specified later), and K is a normalization constant. Note that in Eq. (15) $r_L = p_\perp/m\Omega_e$ is also a constant of motion, and K is to be determined from the condition,

$$\int f_0\, 2\pi r dr d^3p = N, \tag{16}$$

where N is the line density of the electron beam (i.e. number of electrons per unit length).

After some algebra, Eq. (15) can be written

$$f_0 = N\pi^{-1}\,[\delta(\hat{\phi} - \hat{\phi}_0) + \delta(\hat{\phi} - \pi + \hat{\phi}_0)]\; g\;(p_\perp, p_z)\; S\;(r - r_1)\; S\;(r_2 - r)$$
$$\times\; [(r^2 - r_1^2)\;(r_2^2 - r^2)]^{-1/2} \tag{17}$$

where

$$\hat{\phi}_0 = \sin^{-1}\,[(r^2 + r_L^2 - r_0^2)/2rr_L],$$

$$S(x) = \begin{cases} 1, & \text{for } x \geq 0, \\ 0, & \text{for } x < 0, \end{cases}$$

$$r_1 = |r_0 - r_L|,$$

$$r_2 = r_0 + r_L,$$

and g $(p_\perp, p_z)$ satisfies the normalization condition.

$$2\pi \int_0^\infty p_\perp\, dp_\perp \int_{-\infty}^{\infty} dp_z\; g\;(p_1, p_z) = 1.$$

Equation (17) specifies an electron beam in which all electrons have the same guiding center position $(r_0)$. Through a simple super position procedure (e.g. specifying a weighing

function of $r_0$ and carrying out an integration over $r_0$), Eq. (17) can be readily extended to treat a beam with a spread in electron guiding center positions. In the remaining part of this paper, however, we shall concentrate on a cold monoenergetic beam with no spread in guiding center positions. Thus, we let

$$g\ (p_\perp, p_z)\ = \delta\ (p_\perp - p_{\perp o})\delta\ (p_z\ - p_{zo})/2\pi p_\perp, \tag{18}$$

where $p_{\perp o}$ and $p_{zo}$ are, respectively, the perpendicular and parallel momenta of the electrons.

Equation (17) together with Eq. (18) is an idealized representation of the magnetron-type electron beam commonly used in cyclotron maser experiments[35–37,41]. From the analytical point of view, such a distribution function has some advantages. First, it leads to results which can be physically interpreted. Second, it gives simple analytical formulas for the determination of optimum beam positions and energies. Finally, it serves as the basis of super position for forming a beam with arbitrary thermal and guiding center spreads. One notes that the method of super position is applicable here because the self fields of the beam have been neglected.

## IV. RESULT

### A. Beam power gain

Combining Eqs. (2), (11), (12), (13), (17) and (18), we obtain an explicit expression for the time averaged beam power gain,

$$P = P_1 + P_2 + P_3 + P_4 \tag{19}$$

where

$$P_1 = \nu c^2 E_{\theta 0}^2 \tau (8\gamma_0 \omega)^{-1} \sum_{s=-\infty}^{\infty} \Big\{ - H_s(k_n r_0, k_n r_L) \tau \beta_{\perp 0}^2 \Delta^{-3} \{ (\omega^2 - k_z^2 c^2) L \cdot [2(1 - \cos\Delta) - \Delta \sin\Delta] + k_z c^2 \Delta (\Delta \sin\Delta + \cos\Delta - 1) \} + Q_s(k_n r_0, k_n r_L) L \Delta^{-2} (\omega - k_z v_{z0}) (1 - \cos\Delta) \Big\}, \tag{20}$$

$$P_2 = \nu c^2 E_{\theta 0}^2 \tau (8\gamma_0 \omega)^{-1} \sum_{s=-\infty}^{\infty} \Big\{ H_s(k_n r_0, k_n r_L) \tau \beta_{\perp 0}^2 \Delta^{-2} \Delta'^{-1} \{ [(\omega^2 - k_z^2 c^2) L \cdot [(1 - \cos\Delta')(1 + \Delta\Delta'^{-1}) - \Delta \sin\Delta'] + k_z c^2 \Delta [\Delta \sin\Delta' - \Delta\Delta'^{-1} (1 - \cos\Delta')] \} - Q_s(k_n r_0, k_n r_L) L \Delta^{-1} \Delta'^{-1} (\omega - k_z v_{z0}) (1 - \cos\Delta') \Big\}, \tag{21}$$

$$\nu \equiv Ne^2/mc^2,$$

$$\gamma_0 \equiv [1 + (p_{\perp 0}^2 + p_{z0}^2)/m^2 c^2]^{1/2},$$

$$\beta_{\perp 0} \equiv p_{\perp 0}/\gamma_0 mc,$$

$$v_{z0} \equiv p_{z0}/\gamma_0 m,$$

$$\tau \equiv L/v_{z0},$$

$$\Delta \equiv (\omega - k_z v_{z0} - s\Omega_e/\gamma_0)\tau,$$

$$\Delta' \equiv (\omega + k_z v_{z0} - s\Omega_e/\gamma_0)\tau,$$

the functions $P_3$ and $P_4$ are similarly defined as $P_1$ and $P_2$, respectively, but with $\omega$ replaced by $-\omega$, $\Delta$ replaced by $-\Delta'$, and $\Delta'$ replaced by $-\Delta$. Finally, the double-argument functions

$H_s$ and $Q_s$ in Eqs. (20) and (21) are defined as

$$H_s(a_0, a_L) \equiv J_s'(a_L) I_s(a_0, a_L), \tag{23}$$

$$Q_s(a_0, a_L) \equiv 2H_s(a_0, a_L) + a_L J_s''(a_L) I_s(a_0, a_L) + \frac{1}{2} a_L J_s'(a_L) [I_{s-1}(a_0, a_L) - I_{s+1}(a_0, a_L)], \tag{24}$$

where

$$I_s(a_0, a_L) \equiv -\frac{2}{\pi} \int_{a_1}^{a_2} da J_1(a) a \sin\phi [(a^2 - a_1^2)(a_2^2 - a^2)]^{-1/2} \cdot \sum_{s'=-\infty}^{\infty} J_{s+s'}(a_L) J_{s'}(a) \cos s' \left(\frac{\pi}{2} - \phi\right), \tag{25}$$

$$a_1 \equiv |a_0 - a_L|,$$

$$a_2 \equiv a_0 + a_L,$$

$$\phi \equiv \sin^{-1}[(a^2 + a_L^2 - a_0^2)/(2aa_L)].$$

The integral series in Eq. (24) has been evaluated in Appendix A with the result

$$I_s(a_0, a_L) = J_s^2(a_0) J_s'(a_L). \tag{26}$$

Substituting Eq. (26) into Eqs. (23) and (24), we obtain

$$H_s(a_0, a_L) = [J_s(a_0) J_s'(a_L)]^2, \tag{27}$$

$$Q_s(a_0, a_L) = 2H_s(a_0, a_L) + a_L J_s'(a_L) J_s''(a_L) \{J_s^2(a_0)(1 + s^2/a_0^2) + [J_s'(a_0)]^2\} + 2s^2 J_s(a_0) J_s'(a_0) J_s'(a_L) [a_L J_s'(a_L) - J_s(a_L)]/a_0 a_L.$$

We assume that in actual operations, radiation at a particular cyclotron frequency is favored, i.e. the parameters will be so chosen that only one term on the right hand side of Eq. (20) or (21) dominates. Hence we will drop the summation signs in Eqs. (20) and (21).

**B. Physical interpretation of the beam-wave coupling coefficient $H_s(k_n r_0, k_n r_L)$**

In Eq. (20) or (21), the first term (i.e. the term proportional to $\beta_{\perp 0}^2$ and $H_s$) originates from the transverse motion of the electrons. This is the source term for the cyclotron maser radiation. It can be either positive (beam power gain) or negative (beam power loss) depending primarily on the value of the phase factor $\Delta$. The second term (proportional to $Q_s$) originates from wave induced oscillations. It is a positive term, hence leads to beam power gain. However, unless the beam transverse velocity $\beta_{\perp 0}$ is too low to be of practical interest, it is always insignificant when compared with the first term. Thus, for practical purposes, the beam power gain is proportional to $H_s(k_n r_0, k_n r_L)$, which will henceforth be referred to as the beam-wave coupling coefficient. The physical significance of $H_s$ can be understood as follows. Consider the projection of an electron orbit on the cross-sectional plane of the cavity as shown in Fig. 4, where point $O$ is the axis of symmetry, point $e$ is the position of an arbitrarily chosen electron, point $C$ is the guiding center of this electron, and the circle of radius $r_L$ is its cyclotron orbit. The electron $e$ loses or gains energy in the cavity fields through its interaction with $E_\phi$, the component of the cavity electric field tangential to the electron cyclotron orbit, i.e.

$$\begin{aligned} E_\phi &= E_\theta \cos\alpha \\ &= E_{\theta 0} J_1(k_n r) \cos\alpha, \end{aligned} \tag{28}$$

where the $z$-dependence of $E_\phi$ has been neglected. We may express $E_\phi$ in terms of $r_0$, $r_L$, and $\phi$ through the following geometrical relations (see Fig. 4):

$$r = (r_0^2 + r_L^2 - 2 r_0 r_L \cos\phi)^{1/2}$$

$$\cos\alpha = [r_L + r_0 \cos(\pi - \phi)]/r$$

$$= (r_L - r_0 \cos\phi)/(r_0^2 + r_L^2 - 2 r_0 r_L \cos\phi)^{1/2}$$

Thus,

$$E_\phi = E_{\theta 0} J_1 [k_n (r_0^2 + r_L^2 - 2r_0 r_L \cos\phi)^{1/2}] (r_L - r_0 \cos\phi)$$

$$\cdot [r_0^2 + r_L^2 - 2r_0 r_L \cos\phi]^{-1/2}$$

$$= - E_{\theta 0} k_n^{-1} \frac{\partial}{\partial r_L} J_0 [k_n (r_0^2 + r_L^2 - 2r_0 r_L \cos\phi)^{1/2}]. \tag{29}$$

Expanding $E_\phi$ in terms of the sinusoidal harmonics of $\phi$ and noting that $E_\phi$ is an even function of $\phi$, we obtain

$$E_\phi = \sum_{s=0}^{\infty} E_{eff}^s \cos s\phi \tag{30}$$

where

$$E_{eff}^s = \frac{\Theta}{\pi} \int_0^\pi d\phi E_\phi \cos s\phi$$

$$= - \Theta E_{\theta 0} (k_n \pi)^{-1} \frac{\partial}{\partial r_L} \int_0^\pi d\phi J_0 [k_n (r_0^2 + r_L^2 - 2r_0 r_L \cos\phi)^{1/2}], \tag{31}$$

$$\Theta = \begin{cases} 1, & s = 0 \\ 2, & s \neq 0. \end{cases}$$

Using tabulated integral formulae,[44] we obtain from Eq. (31),

$$E_{eff}^s = - \Theta E_{\theta 0} J_s (k_n r_0) J_s' (k_n r_L).$$

$$= - \Theta E_{\theta 0} H_s^{1/2} (k_n r_0, k_n r_L) \tag{32}$$

The coefficient $E_{eff}^s$ is the amplitude of the $s$-th harmonic component of the wave electric field in the direction of the electron velocity. This is the component which provides the effective electric field for beam-wave coupling at the $s$-th cyclotron harmonic frequency. The beam power gain scales with the square of $E_{eff}^s$, which explains why it is proportional to $H_s (k_n r_0, k_n r_L)$. One notes that even if the actual electric field ($E_{\theta 0}$) is large, the effective electric field ($E_{eff}^s$) for higher harmonic interactions ($s > 1$) may be small because it is proportional to $H_s^{1/2} (k_n r_0, k_n r_L)$. From Eqs. (27) and (32), it is easily seen that $E_{eff}^s$ for $s > 1$ actually

vanished as $r_L \to 0$. This is expected because non-fundamental cyclotron harmonic interactions result from the finite Larmor radius effect.

### C. Normalization

It is convenient to introduce a normalization scheme by which the cavity radius $r_w$ is scaled out of the results. This can be achieved through the following procedures (normalized notations are denoted by a bar):

(i) length normalized to $r_w$ (e.g. $\bar{r}_0 = r_0/r_w$);

(ii) frequency normalized to $c/r_w$ (e.g. $\bar{\omega} = \omega r_w/c$);

(iii) momentum normalized to $mc$ (e.g. $\bar{p}_{\perp 0} = p_{\perp 0}/mc$); and

(iv) EM fields normalized to $mc^2/er_w$ (e.g. $\bar{E}_{\theta 0} = E_{\theta 0} er_w/mc^2$).

Other quantities such as $k_z$ and $\tau$ are to be normalized consistently with the preceeding procedures (e.g. $\bar{k}_z = k_z r_w$, $\bar{\tau} = \tau c/r_w$). However, naturally dimensionless quantities such as $\gamma_0$, $\nu$, $\Delta$, $H_s$ and $Q_s$ will remain unchanged.

### D. Optimization of guiding center position

In the beam power gain function P [Eq. (19)] one finds that the guiding center position $\bar{r}_0$ only appears is the beam-wave coupling coefficient $H_s(x_n\bar{r}_0, x_n\bar{r}_L)$, where the arguments $x_n\bar{r}_0$ and $x_n\bar{r}_L$ are, respectively, the normalized forms of $k_n r_0$ and $k_n r_L$. Therefore, to maximize P with respect to $\bar{r}_0$, one only needs to find the value(s) of $\bar{r}_0$ which maximizes $H_s$. We now examine the behavior of $H_s(x_n\bar{r}_o, x_n\bar{r}_L)$ as a function of its arguments. Figures 5a, b, c, and d show the surface plots of $H_s$ versus $x_n\bar{r}_0$ and $x_n\bar{r}_L$ for the first four cylotron harmonics. We note that the regime $x_n\bar{r}_L > s$ is of no interest because the condition of frequency synchrony ($\omega - k_z v_{zo} \simeq s\Omega_e/\gamma_0$) is not satisfiable there. From Fig. 5 and Eq. (27), we observe the following properties of $H_s$: (i) the height of $H_s$ dereases as s increases; (ii) $H_s$ is a decreasing function of $x_n\bar{r}_L$ for $s = 1$ and an increasing function of $x_n\bar{r}_L$ for $s > 1$; and (iii) $H_s$ is a

nonmonotonic function of $x_n\bar{r}_0$ with an infinite number of peaks. The first peak is the largest and the subsequent ones are successively smaller. Note that the peaks of $H_s$ do not in general coincide with those of $E_\theta$ except for s = 1. Given a fixed value of n, there are values of $\bar{r}_0$ for which $H_s$ vanishes. Evidently, it is important to select $\bar{r}_0$ such that $H_s$ falls on or near one of its peaks with respect to $x_n\bar{r}_0$. Tables I, II, and III list the values of $\bar{r}_0$ corresponding to the first three peaks of $H_s$ for various combinations of *s* and *n*. For a given combinatin of s and n, the value of $\bar{r}_0$ listed on Table I is more preferable to those on Tables II and III because it corresponds to the first peak of $H_s$.

### E. Total beam energy gain during one transit time

The total stored field energy ($W_f$) in the cavity is given by

$$W_f = E_{\theta 0}^2 \, r_w^2 \, J_0^2 \, (x_n) L/16. \tag{33}$$

It is convenient to introduce a dimensionless quantity $F$ defined as the ratio of the total beam energy gain during one transit time to the total stored field energy, i.e.

$$F \equiv P_T / W_f. \tag{34}$$

substituting Eqs. (19) and (33) into Eq. (34), we obtain

$$F = 2 \, \nu \bar{\tau}^2 \, [\gamma_0 \, J_0^2 \, (x_n) \, \bar{\omega}]^{-1} \, (\alpha_1 + \alpha_2 + \alpha_3 + \alpha_4), \tag{35}$$

where

$$\begin{aligned} \alpha_1 = & - H_s \, \beta_{\perp 0}^2 \, \bar{\tau} \, \Delta^{-3} \, [(\bar{\omega}^2 - \bar{k}_z^2) \, (4 \sin^2 \Delta/2 - \Delta \sin \Delta) \\ & + \bar{k}_z \, \bar{L}^{-1} \, \Delta \, (\Delta \sin \Delta - 2 \sin^2 \Delta/2)] \\ & + 2 Q_s \, \Delta^{-2} \, (\bar{\omega} - \bar{k}_z \beta_{z0}) \sin^2 \Delta/2, \end{aligned} \tag{36a}$$

$$\alpha_2 = H_s \, \beta_{\perp 0}^2 \, \bar{\tau} \, \Delta^{-2} \, \Delta'^{-1} \, [(\bar{\omega}^2 - \bar{k}_z^2) \, [2 \, (1 + \Delta/\Delta') \sin^2 \Delta'/2 - \Delta \sin \Delta']$$

$$+ \bar{k}_z \bar{L}^{-1} \Delta \ (\Delta \sin \Delta' - 2\Delta\Delta'^{-1} \sin^2 \Delta'/2)\}$$

$$- 2Q_s \ \Delta^{-1}\Delta'^{-1} \ (\bar{\omega} - \bar{k}_z \beta_{z0}) \sin^2 \Delta'/2, \tag{36b}$$

$$\alpha_3 = - H_s \beta_{\perp 0}^2 \ \bar{\tau} \ \Delta'^{-3} \ [(\bar{\omega}^2 - \bar{k}_z^2) \ (4 \sin^2 \Delta'/2 - \Delta' \sin \Delta')$$

$$- \bar{k}_z \bar{L}^{-1} \Delta' (\Delta' \sin \Delta' - 2 \sin^2 \Delta'/2)]$$

$$+ 2Q_s \ \Delta'^{-2} \ (\bar{\omega} + \bar{k}_z \beta_{z0}) \sin^2 \Delta'/2, \tag{36c}$$

$$\alpha_4 = H_s \beta_{\perp 0}^2 \ \bar{\tau} \ \Delta^{-1}\Delta'^{-2}\{(\bar{\omega}^2 - \bar{k}_z^2) \ [2 \ (1 + \Delta'/\Delta) \sin^2 \Delta/2 - \Delta' \sin \Delta]$$

$$- \bar{k}_z \ \bar{L}^{-1} \ \Delta' \ (\Delta' \sin \Delta - 2\Delta' \Delta^{-1} \sin^2 \Delta/2)\}$$

$$- 2Q_s \Delta\Delta'^{-1} \ (\bar{\omega} + \bar{k}_z \beta_{z0}) \sin^2 \Delta/2, \tag{36d}$$

*and the arguments of $H_s$ and $Q_s$ are $x_n \bar{r}_0$ and $x_n \bar{r}_L$.*

If we decompose the cavity standing wave into a forward travelling wave and a backward travelling wave, then in Eq. (8), $f_+^{(1)}$ and $f_-^{(1)}$ are the beam perturbations due to the forward and backward travelling waves, respectively. Similarly in Eq. (35), $\alpha_1$, $\alpha_2$ are due to the interactions of $f_+^{(1)}$ with the forward and backward travelling waves, respectively, and $\alpha_3$ , $\alpha_4$ are due to the interactions of $f_-^{(1)}$ with the backward and forward travelling waves, respectively.

In order for the beam to generate, rather than absorb, electromagnetic radiation, it is important to match parameters so that $F$ assumes negative values. The sign of $F$ is principally determined by the phase factor $\Delta$. Figure 6 shows a typical plot of $F$ as a function of $\Delta$ (solid curve, marked by $F$). The four components of $F$ represented by the four terms in Eq. (35) are also ploted (dashed curves marked by 1, 2, 3, and 4). It is seen from the plot of $F$ that negative beam energy gain occurs when

$$- \pi/2 \leqslant \Delta \leqslant 2\pi. \tag{37}$$

Eq. (37) gives the resonant wave frequency width ($\delta\omega$) and cyclotron frequency width ($\delta\Omega_e/\gamma_0$) for negative beam energy gain, i.e.

$$\delta\omega \simeq 2\pi/\tau, \tag{38a}$$

and

$$\delta\Omega_e/\gamma_o \simeq 2\pi/s\tau. \tag{38b}$$

One notes, however, that the frequency band width of a cavity eigenmode (see item F of this section) is usually much narrower than that given by Eq. (38a).

Equation (35) has been evaluated for a wide range of parameters, all showing the same condition [Eq. (37) or (38)] for negative beam energy gain. However, the maximum negative value of $F$ (point X in Fig. 6) shifts toward smaller $\Delta$ when $\bar{L}$ increases. Also, $F$ increases sharply when $\bar{\tau}$ and $\beta_{\perp 0}$ increase, as expected from the analytical form of $F$. Here we note an important difference between the cyclotron maser interactions in waveguides and cavities. In a waveguide, only one type of interaction is present, namely, the beam and forward travelling wave interaction. It has been shown [1-3] that, for such a case, negative beam energy gain occurs only when $\omega - k_z\beta_{z0} - s\Omega_e/\gamma_0$ ( $= \Delta/\tau$ ) $> 0$. This interaction corresponds to the $\alpha_1$ term of Eq. (35). As shown in Fig. 6, the $\alpha_1$ term indeed assumes negative values only when $\Delta > 0$ (consider only the region $-2\pi < \Delta < 2\pi$ ). In a cavity, the saturation is more complicated because the beam interacts with a standing wave (two oppositely directed travelling waves). Consequently, there are four types of interactions leading to the four terms in Eq. (35), as just pointed out. Furthermore, all four terms are important (see Fig. 6) and when they add up, the net effect is such that negative beam energy gain occurs not only for positive $\Delta$ but for slightly negative $\Delta$ also (see Fig. 6). The differences in the interaction processes may also have important implications in nonlinear considerations. For example, in order to enhance the beam-to-wave energy transfer efficiency in a waveguide, one only has to raise the saturation

level of the beam and forward travelling wave interaction through, for example, magnetic field adjustment [13,14]. In a cavity, however, raising the saturation level of one type of interaction does not necessarily lead to a higher overall efficiency since there are three other types of interactions whose contributions might be adversely affected.

In view of the lengthy algebra involved in the present analysis, an independent check of the results appears warranted. We have developed a numerical code which calculates a single electron orbit (hence its energy change) in the cavity fields of Eqs. (2) to (4). The field amplitude is kept sufficiently low so that orbit perturbations remain linear. Taking an ensemble average over the distribution represented by Eqs. (17) and (18), we then obtain the corresponding values of $F$ from the numerical code, which are shown by dots in Fig. 6. The agreement between the numerical and analytical approaches has been excellent for the case shown and also for a large number of other cases we have checked.

**F. Threshold beam power**

The present model assumes an idealized cavity, namely, a cavity with discrete eigenfrequencies. In practice, a cavity always has a finite $Q$ [defined in Eq. (39)] due to loading or wall resistivity, which leads to narrow bands of eigenfrequencies with width $\sim 2\omega/Q$. From Eq. (38a), we find that the frequency width for negative beam energy gain is approximately $2\pi/\tau$. Thus, a cavity of finite $Q$ can be effectively treated as an idealized cavity if

$$\pi/\tau \gg \omega/Q.$$

This is a condition easily satisfiable even for unusually low values of $Q$ or large values of $\tau$.

Because of finite $Q$, energy is drained from the cavity at the rate

$$P_{out} = \omega W_f/Q, \tag{39}$$

while the beam pumps energy into the cavity at the rate

$$P_{in} = -FW_f/\tau. \tag{40}$$

From the condition of power balance, $P_{in} \geqslant P_{out}$, we obtain a threshold condition for cavity oscillations,

$$-FQ \geqslant \omega\tau \tag{41}$$

The beam power is given by

$$P_b = N(\gamma_0 - 1)mc^2 v_{z0}. \tag{42}$$

Inserting Eq. (35) into Eq. (41) and making use of Eq. (42), we may rewrite Eq. (41) as

$$P_b \geqslant P_b^{Th}$$

where $P_b^{Th}$, the threshold beam power for cavity oscillations, is defined as

$$P_b^{Th} = -\frac{\bar{\omega}^2\beta_{z0}^2\gamma_0(\gamma_0 - 1)J_0^2(x_n)}{Q\bar{L}(\alpha_1 + \alpha_2 + \alpha_3 + \alpha_4)} \frac{m^2c^5}{2 \times 10^{10}e^2}\ kW. \tag{44}$$

In Eq. (44), $c$, $e$, and $m$ are to be expressed in Gaussian units, while all other quantities are either normalized or dimensionless.

Equation (44) is a function of nine free parameters, i.e. $s$, $n$, $l$, $\bar{r}_0$, $\bar{L}$, $\gamma_0$, $Q$, $\bar{\Omega}_e$, and the ratio of electron transverse velocity to parallel velocity ($v_{\perp 0}/v_{z0}$). In the numerical data to be presented, we let the radial eigenmode number $n$ equal the cyclotron harmonic number $s$. Such a combination of $n$ and $s$ allows us to choose an optimum $\bar{r}_0$ from Table I (see the numbers marked by *) which is approximately halfway between the cavity wall and the axis. The axial eigenmode number $l$ will be fixed at $l = 1$. With $s$, $n$, and $l$ known, the cavity eigenfrequency $\bar{\omega}$ can be calculated. The cyclotron frequency $\bar{\Omega}_e$ will be so specified that the beam energy loss is a maximum with respect to $\Delta$ (see point $X$ on Fig. 6). The velocity ratio will be fixed at $v_{\perp 0}/v_{z0} = 1.5$, which is consistent with most experimental conditions. Finally, $Q$ and $P_b^{Th}$ can be combined into a single parameter. The remaining parameters $s$, $\bar{L}$, and $\gamma_0$ will be varied. Note that the cavity wall radius $r_w$ has been scaled out of the final results. Figures 7a, b, and c

plot $QP_b^{Th}$ as a function of the electron kinetic energy $W_b$, where $W_b = (\gamma_0 - 1)mc^2$, for the first four cyclotron harmonics and for $\bar{L} = 5$, 10, and 20. It is seen that, for a fixed $Q$, the first cyclotron harmonic can be excited with the lowest threshold beam power $P_b^{Th}$, and the higher the beam energy, the higher $P_b^{Th}$ becomes. For higher cyclotron harmonics, on the other hand, $P_b^{Th}$ is considerably higher, but there is an optimum beam energy for which $QP_b^{Th}$ is lowest. Although $P_b^{Th}$ can be lowered by increasing either $Q$ or $\bar{L}$, for reasonable values of $Q$ and $\bar{L}$, it still requires a relatively high electron energy and beam power to excite cyclotron harmonics above 2. As an example, we apply the present results to the experiments of Kisel et. al.[35] Using their parameters ($Q \simeq 4000$, $\bar{L} \simeq 7$, and $W_b \simeq 20$ keV), we find from Eq. (44) [or approximately by interpolating from Figs. 7(a) and (b)] that $P_b^{Th}$ for the first, second, third and fourth cyclotron harmonics are, respectively, 1.5 kW, 22.1 kW, 297.5 kW, and 3800 kW. Thus, their beam power ($\leqslant$ 70 kW) was sufficient to excite the first and second cylotron harmonics (as reported in their paper) but far below the necessary power to excite the third and fourth cyclotron harmonics. It is also found from Eq. (44) that their beam energy ($\sim$ 20 keV) is very close to the optimum energy (i.e. the energy that requires the lowest threshold beam power) for exciting the second harmonic but is a factor of 3 and 8 below the optimum energies for the third and fourth cyclotron harmonics, respectively.

## V. DISCUSSION

We first consider the validity of the linear approximation. In solving the Vlasov equation, we have made the assumption (in Gaussian units)

$$E_{\theta 0} \ll B_0 \tag{45}$$

Making use of Eqs. (33) and (39), this assumption can be rewritten as a condition on the output power $P_{out}$

$$QP_{out} \ll \frac{1}{16} B_0^2 r_w^2 J_0^2 (x_n) \omega L, \tag{46}$$

where $P_{out}$ is the sum of the output wave power and the power dissipated in walls. This condition is generally well satisfied at the threshold beam power level. As a numerical example, we use the parameters of Fig. 6 and assume $r_w = 1$ cm, then Eq. (46) gives

$$QP_{out} \ll 3\times 10^7 \, kW \tag{47}$$

For the same parameters, $QP_b^{Th}$ is only $5\times 10^4 \, kW$ (see Fig. 7a).

Using Eq. (37), we may derive a validity condition for the cold beam assumption. Equation (37) shows that the range of $\Delta$ for negative beam energy gain is approximatly $2.5\pi$, where $\Delta$ has been defined as

$$\Delta = (\bar{\omega} - \bar{k}_z \beta_{z0} - s\bar{\Omega}_e/\gamma_0)\bar{\tau}. \tag{48}$$

Thus, if

$$(\bar{k}_z \, \delta\beta_z + s\bar{\Omega}_e \, \delta\gamma/\gamma_0^2) \, \bar{\tau} \ll 2.5\pi, \tag{49}$$

where $\delta\beta_z$ and $\delta\gamma$ are, respectively, the axial velocity spread and energy spread, the cold beam assumption is essentially valid. Since $\bar{k}_z = l\pi/\bar{L}$ and $\bar{\tau} = \bar{L}/\beta_{z0}$, we may rewrite condition (49) as

$$(l\pi\delta\beta_z + s\bar{\Omega}_e \bar{L}\,\delta\gamma/\gamma_0^2)/\beta_{z0} \ll 2.5\pi. \tag{50}$$

Thus, the condition becomes more restrictive as the axial eigenmode number ($l$), the cavity length ($\bar{L}$), and the wave frequency ($- s\bar{\Omega}_e/\gamma_o$) increase or as the beam axial velocity ($\beta_{z0}$) decreases.

Turning to nonlinear considerations, we can obtain a crude estimate of the limiting cavity length beyond which the energy conversion efficiency begins to drop. Equation (37) gives the approximate range of $\Delta$ for which the beam will lose energy in traversing the cavity, where in the linear analysis $\Delta$ has been defined in Eq. (48). Since Eq. (37) is a phase synchrony condition, we expect it to hold true in the nonlinear stages of the interaction as well. In which case we replace the initial energy $\gamma_0$ in Eq. (48) with the instantaneous energy $\gamma$ and note that $\beta_{z0}$ remains relatively constant because of the absence of any axial electric field. Assuming $<\gamma_f>$ is the average electron energy after leaving the cavity, then the average change of $\Delta$ due to the change of $\gamma$ is approximately $s\Omega_e(<\gamma_f>^{-1} - \gamma_0^{-1})$. Thus condition (37) can be written

$$s\bar{\Omega}_e\bar{\tau}(\gamma_0 - <\gamma_f>)/\gamma_0 <\gamma_f> \leqslant 2.5\pi \tag{51}$$

Letting $\eta \equiv (\gamma_0 - <\gamma_f>)/(\gamma_0 - 1)$ be the energy conversion efficiency, and writting $\bar{L} = \beta_{z0}\bar{\tau}$, we obtain from Eq. (51)

$$\bar{L} \leqslant \bar{L}_c \equiv \frac{3\pi\beta_{z0}\gamma_0[\gamma_0 - \eta(\gamma_0 - 1)]}{s\bar{\Omega}_e\eta(\gamma_0 - 1)} \tag{52}$$

Equation (52) gives the limiting cavity length $\bar{L}_c$ for achieving maximum efficiency. Note that $\bar{L}_c$ decreases as the efficiency and wave frequency increase or as the beam axial velocity decreases. Thus, while it is possible to lower the threshold beam power by increasing the cavity length, this may also lower the efficiency if condition (52) is violated.

The author would like to thank Dr. A. T. Drobot, Dr. T. Godlove, Dr. V. L. Granatstein,

Dr. M. Read, Dr. J. Silverstein, and Dr. P. Sprangle for many helpful discussions. This work was supported by the Naval Electronic Systems Command. Task PDM3012 and by the Army Ballistic Missile Defense Advanced Technology Center, MIPR W31RPD-83 Z 107.

## REFERENCES

1. R. Q. Twiss, Australian J. Phys. **11**, 564 (1958).
2. J. Schneider, Phys. Rev. Lett. **2**, 504 (1959).
3. A. V. Gaponov, Izv. Vyssh, Uchebn. Zaved., Radiofizika **2**, 450 (1959) and "Addendum," Izv. Vyssh. Uchebn. Zaved., Radiofizika **2**, 837 (1959).
4. V. A. Flyagin, A. V. Gaponov, M. I. Petelin, and V. K. Yulpata, IEEE Trans. Microwave Theory Tech. **25**, 514 (1977).
5. J. L. Hirshfield and V. L. Granatstein, IEEE Trans. Microwave Theory Tech. **25**, 522 (1977).
6. V. V. Alikaev, G. A. Bobrovskii, V. I. Poznyak, K. A. Razumova, V. V. Sannikov, Yu. A. Sokolov, and A. A. Shmarin, Fiz. Plazmy **2**, 390 (1976), [Sov. J. Plasma Phys. **2**, 212 (1976)].
7. J. L. Hirshfield and J. M. Wachtel, Phys. Rev. Lett. **12**, 533 (1964).
8. K. K. Chow and R. H. Pantell, Proc. IRE **48**, 1865 (1960).
9. A. V. Gaponov and V. K. Yulpatov, Radio Eng. Electron Phys. **12**, 582 (1967).
10. Yu. V. Bykov, A. V. Gaponov, and M. I. Petelin, Radio Phys. Quantum Electron **17**, 928 (1974).
11. E. Ott and W. M. Manheimer, IEEE Trans. Plasma Sci. PS-3, 1 (1975).

12. P. Sprangle and W. M. Manheimer, Phys. Fluids **18**, 224 (1975).

13. P. Sprangle and A. T. Drobot, IEEE Trans. Microwave Theory Tech. **25** 528 (1977).

14. K. R. Chu, A. T. Drobot, V. L. Granatstein, and J. L. Seftor, IEEE Trans. Microwave Theory Tech. (to be published).

15. K. R. Chu and J. L. Hirshfield, Phys. Fluids (in press, March, 1978).

16. B. Etlicher, A. Huetz, J. M. Buzzi, P. Haldenwang, and D. Lequeau, to be published.

17. J. L. Hirshfield, I. B. Bernstein and J. M. Wachtel, J. Quantum Electron., Vol. QE-**1**, 237 (1965).

18. T. W. Hsu and P. N. Robson, Electron. Lett. **1**, 84 (1965).

19. A. V. Gaponov, M. I. Petelin, and V. K. Yulpatov, Izv. Vyssh. Uchebn. Zaved., *Radiofizika* ***10***, *1414 (1967). [Radio Phys. Quantum Electron.* ***10***, *794 (1967)]*.

20. G. N. Rapoport, A. K. Nemak, and V. A. Zhurakhovskiy, Radio Eng. Electron. Phys. **12**, 587 (1967).

21. A. F. Kurin, Radio Eng. Electron. Phys. **14**, 1652 (1969).

22. GJ. Sehn and R.E. Hayes, IEEE Trans. Electron Devices (Corresp.) ED-**16**, 1077 (1969).

23. P.A. Lindsay, in Seventh Int. Conf. Microwave and Optical Generation and Amplification, Amsterdam, Holland, Sept. 1970.

24. B. Kulke, IEEE Trans. ED-**19**, 71 (1972).

25. S. V. Kolosov and A. A. Kurayev, Radio Eng. and Electron. Phys. **19**, No. 10, 65 (1974).

26. A. A. Kurayev, F. G. Schevchenko, and V. P. Shestakovich, Radio Eng. and Electron. Phys. **19**, No. 5, 96 (1974).

27. V. L. Bratman and A. E. Tokarev, Izv. Vyssh. Uchebn. Zaved. Radiofiz. **17**, 1224 (1974). [Radio Phys. Quantum Electron **17**. 932 (1974)].

28. M. I. Petelin and V. K. Yulpatov, Radio Phys. Quantum Electron. **18**, 212 (1975).

29. J. B. Bott, Phys. Lett. **14**, 293 (1965).

30. R. L. Schriever and C. C. Johnson, Proc. IEEE **54**, 2029 (1966).

31. J. M. Wachtel and J. L. Hirshfield, Phys. Rev. Lett. **17**, 348 (1966).

32. F. A. Korolev and A. F. Kurin, Radio Eng. Electron. Phys. **15**, 1868 (1970).

33. M. Friedman, D. A. Hammer, W. M. Manheimer, and P. Sprangle, Phys. Rev. Lett. **31**, 752 (1973).

34. Y. Carmel and J. A. Nation, Phys. Rev. Lett. **31**, 806 (1973).

35. D. V. Kisel', G. S. Korablev, V. G. Navel'yev, M. I. Petelin, and Sh. Ye. Tsimring. Radio Eng. Electron. Phys. **19**, No. 4, 95 (1974).

36. N. I. Zaytsev, T. B. Pankratova, M. I. Petelin and V. A. Flyagin, Radio Eng. and Electron. Phys. **19**, No. 5, 103 (1974).

37. A. V. Gaponov, A. L. Gol'denberg, D. P. Grigor'ev, T. B. Pankratova, M. I. Petelin and V. A. Flyagin, Radio Phys. Quantum Electron. **18**, 204 (1975).

38. V. L. Granatstein, M. Herndon, P. Sprangle, Y. Carmel, and J. A. Nation, Plasma Phys. **17**, 23 (1975).

39. V. L. Granatstein, P. Sprangle, M. Herndon, R. K. Parker, and S. P. Schlesinger, J. Appl. Phys. **46**, 3800 (1975).

40. V. L. Granatstein, P. Sprangle, R. K. Parker, and M. Herndon, J. Appl. Phys. **46**, 2021 (1975).

41. H. R. Jory, Varian Associates, Inc., Report No. RADC-TR-77-210 (Jun 1977, unpublished).

42. J. M. Buzzi, H. J. Doucet, B. Etlicher, P. Haldenwang, A. Huetz, H. Lamain and C. Rouille', to be published.

43. See, for example, D. E. Baldwin, I. B. Bernstein, and M. P. H. Weenink, "Kinetic Theory of Plasma Waves in a Magnetic Field," in *Advances in Plasma Physics*" (Interscience, New York, 1969), Vol. 3, p. 1.

44. M. Abramowitz and I. A. Stegun, "Handbook of Mathematical Functions" (Dover, New York, 1965), p. 363.

45. H. Bateman, "Tables of Integral Transforms" (McGraw-Hill, New York, 1954), Vol. 2, p. 362.

## Appendix A

## EVALUATING THE INTEGRAL SERIES $I_s(a_0, a_L)$

The integral series $I_s(a_0, a_L)$ appearing in Eqs. (22) and (23) is defined as

$$I_s(a_0, a_L) \equiv \frac{-2}{\pi} \int_{a_1}^{a_2} da \sin \phi_0 J_1(a) a[(a^2 - a_1^2)(a_2^2 - a^2)]^{-1/2}$$

$$\cdot \sum_{s'=-\infty}^{\infty} J_{s+s'}(a_L) J_{s'}(a) \cos s' \left(\frac{\pi}{2} - \phi_0\right), \tag{A.1}$$

where

$$a_1 = |a_0 - a_L|,$$

$$a_2 = a_0 + a_L,$$

and

$$\phi_0 = \sin^{-1}[(a^2 + a_L^2 - a_0^2)/2aa_L] \tag{A.2}$$

Inserting Eq. (A.2) into Eq. (A.1) and using the Bessel function identity

$$J_s(w) \cos s\Psi = \sum_{s'=-\infty}^{\infty} J_{s+s'}(u) J_{s'}(v) \cos s'\alpha, \tag{A.3}$$

where $w = (u^2 + v^2 - 2uv \cos \alpha)^{1/2}$ and $\Psi = \cos^{-1}[(u - v \cos \alpha)/w]$, we reduce Eq. (A.1) to (after some algebra)

$$I_s(a_0, a_L) = -\frac{J_s(a_0)}{\pi} \int_{a_1}^{a_2} da \frac{J_1(a)(a^2 + a_L^2 - a_0^2)^2}{a_L[(a^2 - a_1^2)(a_2^2 - a^2)]^{1/2}} \cos\left(s \cos^{-1} \frac{a_L^2 + a_0^2 - a^2}{2a_0 a_L}\right), \tag{A.4}$$

To carry out the integration in Eq. (A.4), we replace the variable of integration a with $x$, where $x$ is defined through the equation

$$a = (a_0^2 + a_L^2 - 2a_0 a_L \cos x)^{1/2}.$$

Again after some algebra, we obtain

$$I_s(a_0, a_L) = -\frac{J_s(a_0)}{\pi}\int_0^{\pi} dx \frac{J_1[(a_0^2 + a_L^2 - 2a_0a_L\cos x)^{1/2}]}{(a_0^2 + a_L^2 - 2a_0a_L\cos x)^{1/2}}$$

$$\cdot (a_L - a_0\cos x)\cos sx$$

$$= \frac{1}{\pi} J_s(a_0)\frac{d}{da_L}\int_0^{\pi} dx J_0[(a_0^2 + a_L^2 - 2a_0a_L\cos x)^{1/2}]\cos sx, \tag{A.5}$$

Using tabulated integral *formula*,[45] we obtain

$$I_s(a_0, a_L) = J_s^2(a_0)J_s'(a_L). \tag{A.6}$$

Table I — Values of $\bar{r}_0$ for which $H_s\ (x_n\bar{r}_0,\ x_n\bar{r}_L)$ falls on its first peak with respect to the argument $x_n\bar{r}_0$. The numbers marked by * have been used to obtain the data presented in Fig. 7.

| n \ s | 1 | 2 | 3 | 4 |
|---|---|---|---|---|
| 1 | 0.48* | 0.80 | | |
| 2 | 0.26 | 0.43* | 0.60 | 0.76 |
| 3 | 0.18 | 0.30 | 0.41* | 0.52 |
| 4 | 0.14 | 0.23 | 0.32 | 0.40* |
| 5 | 0.11 | 0.19 | 0.26 | 0.32 |
| 6 | 0.09 | 0.16 | 0.21 | 0.27 |
| 7 | 0.08 | 0.13 | 0.18 | 0.23 |
| 8 | 0.07 | 0.12 | 0.16 | 0.21 |

Table II — Values of $\bar{r}_0$ for which $H_s\ (x_n\bar{r}_0,\ x_n\bar{r}_L)$ falls on its second peak with respect to the argument $x_n\bar{r}_0$.

| n \ s | 1 | 2 | 3 | 4 |
|---|---|---|---|---|
| 1 | | | | |
| 2 | 0.76 | 0.87 | | |
| 3 | 0.52 | 0.60 | 0.79 | 0.91 |
| 4 | 0.40 | 0.46 | 0.60 | 0.70 |
| 5 | 0.32 | 0.37 | 0.49 | 0.56 |
| 6 | 0.27 | 0.34 | 0.41 | 0.47 |
| 7 | 0.23 | 0.29 | 0.35 | 0.41 |
| 8 | 0.21 | 0.26 | 0.31 | 0.36 |

Table III — Values of $\bar{r}_0$ for which $H_s\ (x_n\bar{r}_0,\ x_n\bar{r}_L)$ falls on its third peak with respect to the argument $x_n\bar{r}_0$.

| n \ s | 1 | 2 | 3 | 4 |
|---|---|---|---|---|
| 1 | | | | |
| 2 | | | | |
| 3 | 0.84 | 0.98 | | |
| 4 | 0.64 | 0.75 | 0.85 | 0.95 |
| 5 | 0.52 | 0.61 | 0.69 | 0.77 |
| 6 | 0.44 | 0.51 | 0.58 | 0.65 |
| 7 | 0.38 | 0.44 | 0.50 | 0.56 |
| 8 | 0.33 | 0.38 | 0.44 | 0.49 |

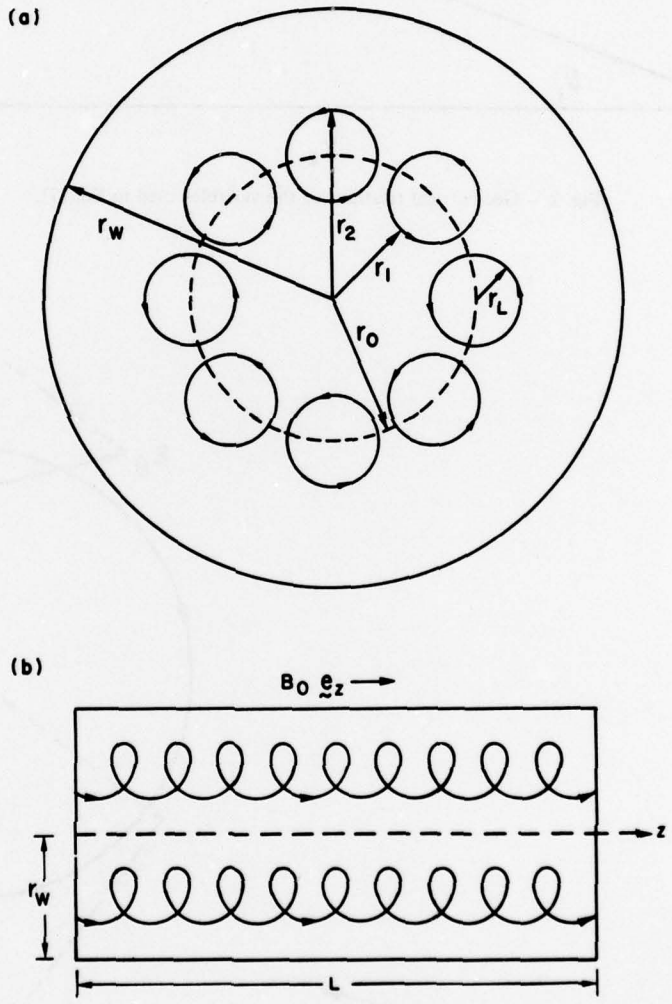


Fig. 1 – (a) End view of the electron cyclotron maser configuration. Guiding centers of all electrons are uniformly distributed on the circle of constant radius $r_0$. The applied magnetic field (not shown) points toward the reader. (b) Side view of the same configuration.

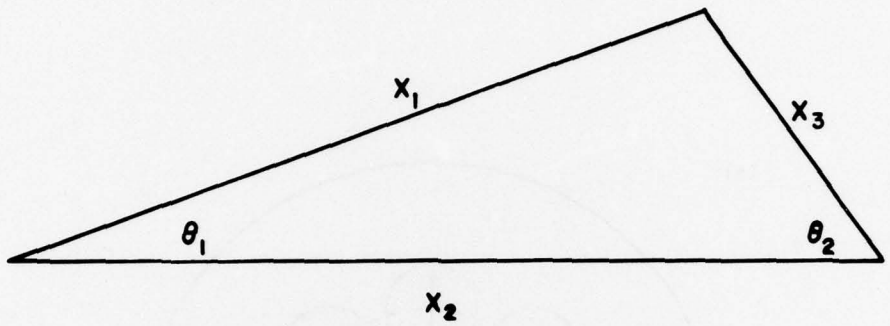


Fig. 2 – Geometrical relations of the variables used in Eq. (7).

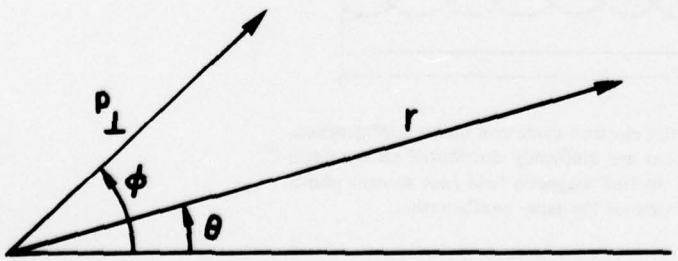


Fig. 3 – Schematic plots of the polar variables ($p_\perp$, $\phi$) and ($r$, $\theta$).

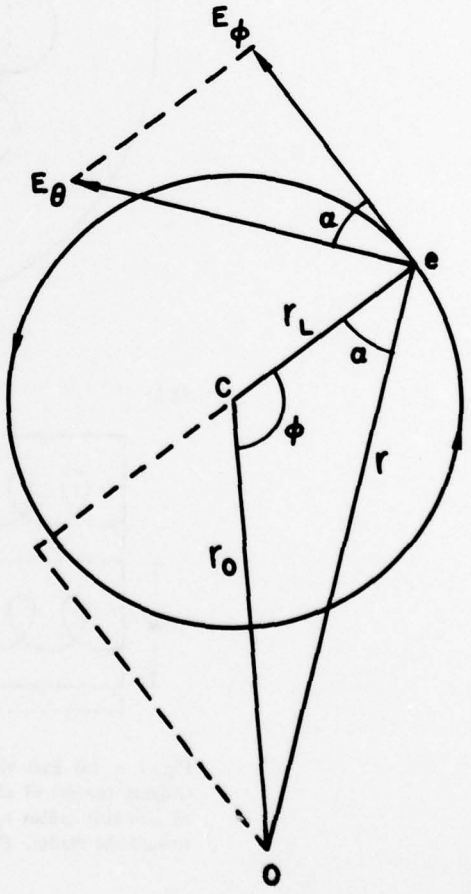


Fig. 4 – Projection of an electron orbin on the cross-sectional plane of the cavity.

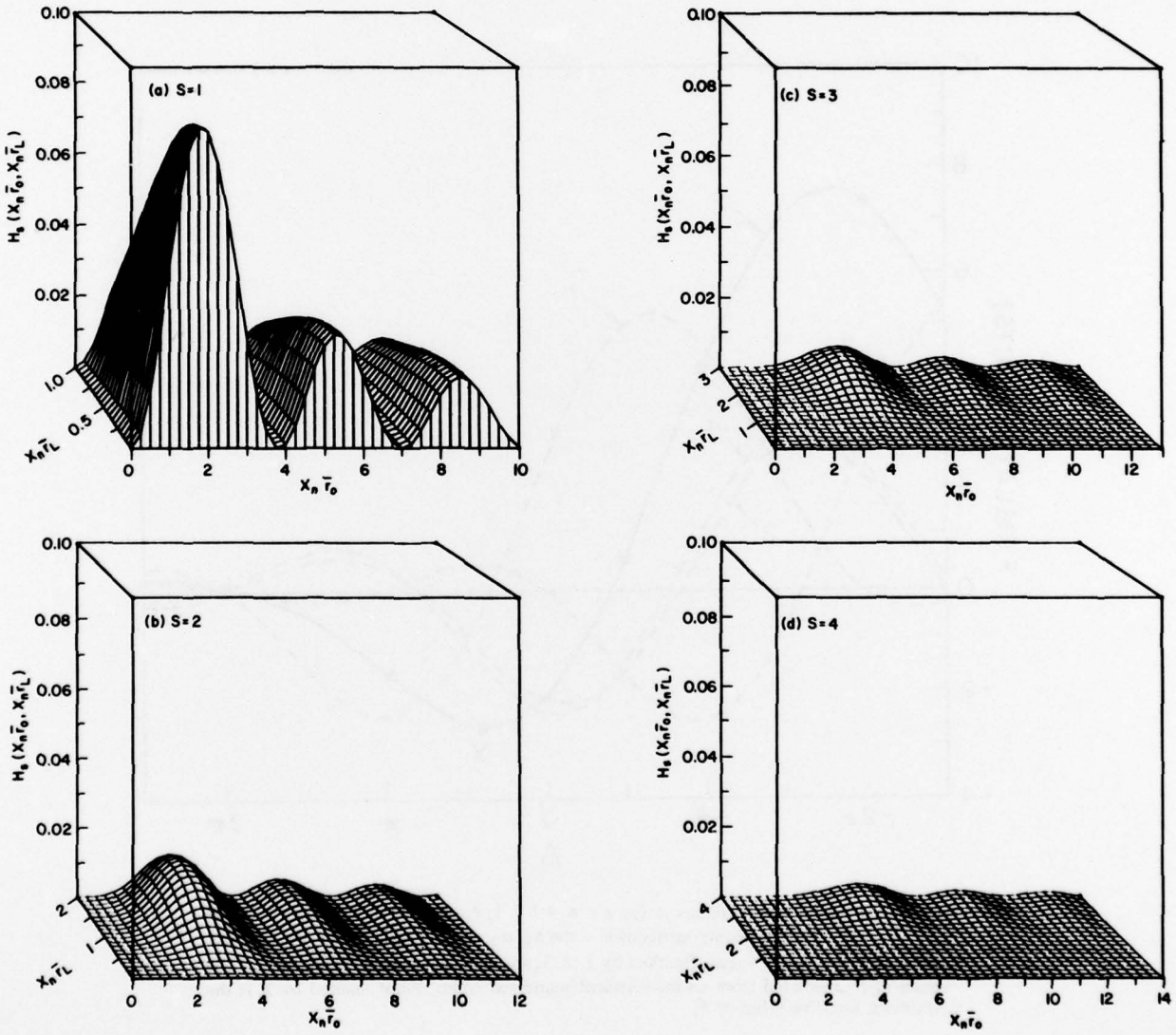


Fig. 5 – Plots of the beam-wave coupling coefficient $H_s(x_n\bar{r}_0, x_n\bar{r}_L)$ as a function of its arguments for the first four cyclotron harmonics.

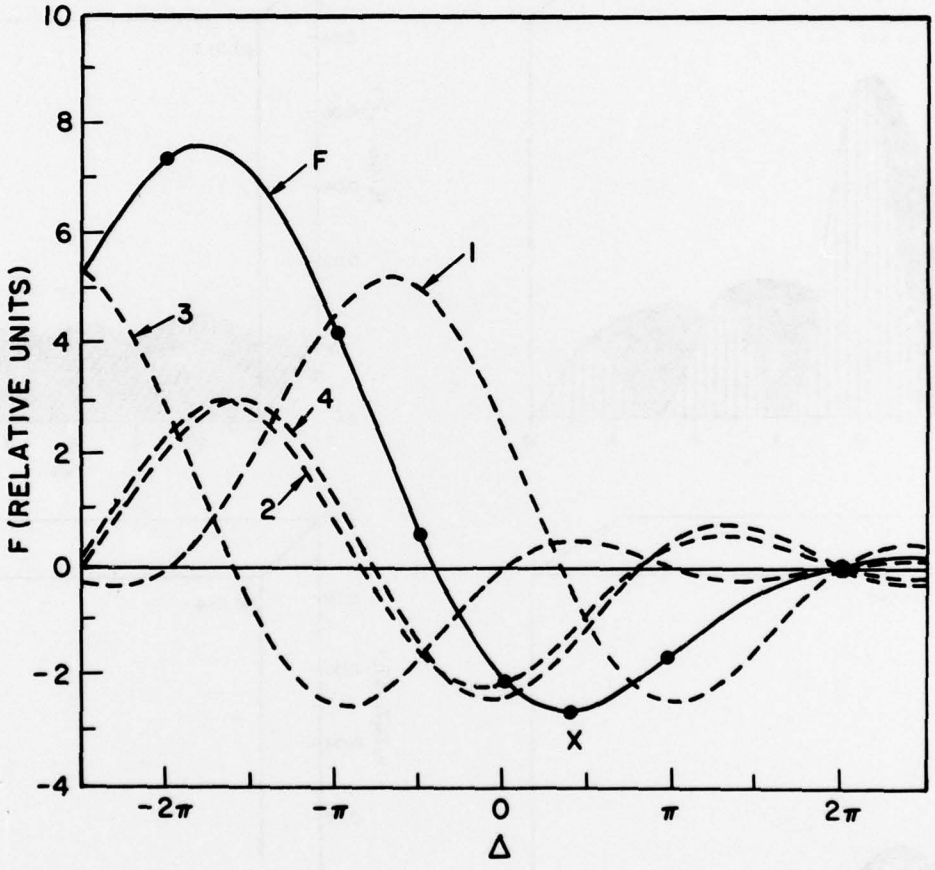


Fig. 6 – $F$ (solid wave) versus $\Delta$ for $s = n = l = 1$, $\bar{r}_0 = 0.48$, $\bar{L} = 5$, $\gamma_0 = 1.1$, and $v_{\perp 0}/v_{z0} = 1.5$. The four components of $F$ – the $\alpha_1$, $\alpha_2$, $\alpha_3$, and $\alpha_4$ terms in Eq. (35)-are also plotted in dashed curves (marked by 1, 2, 3, and 4, respectively). Solid dots are the values of $F$ calculated from an independent numerical code. Point marked by X is the maximum negative value of $F$,

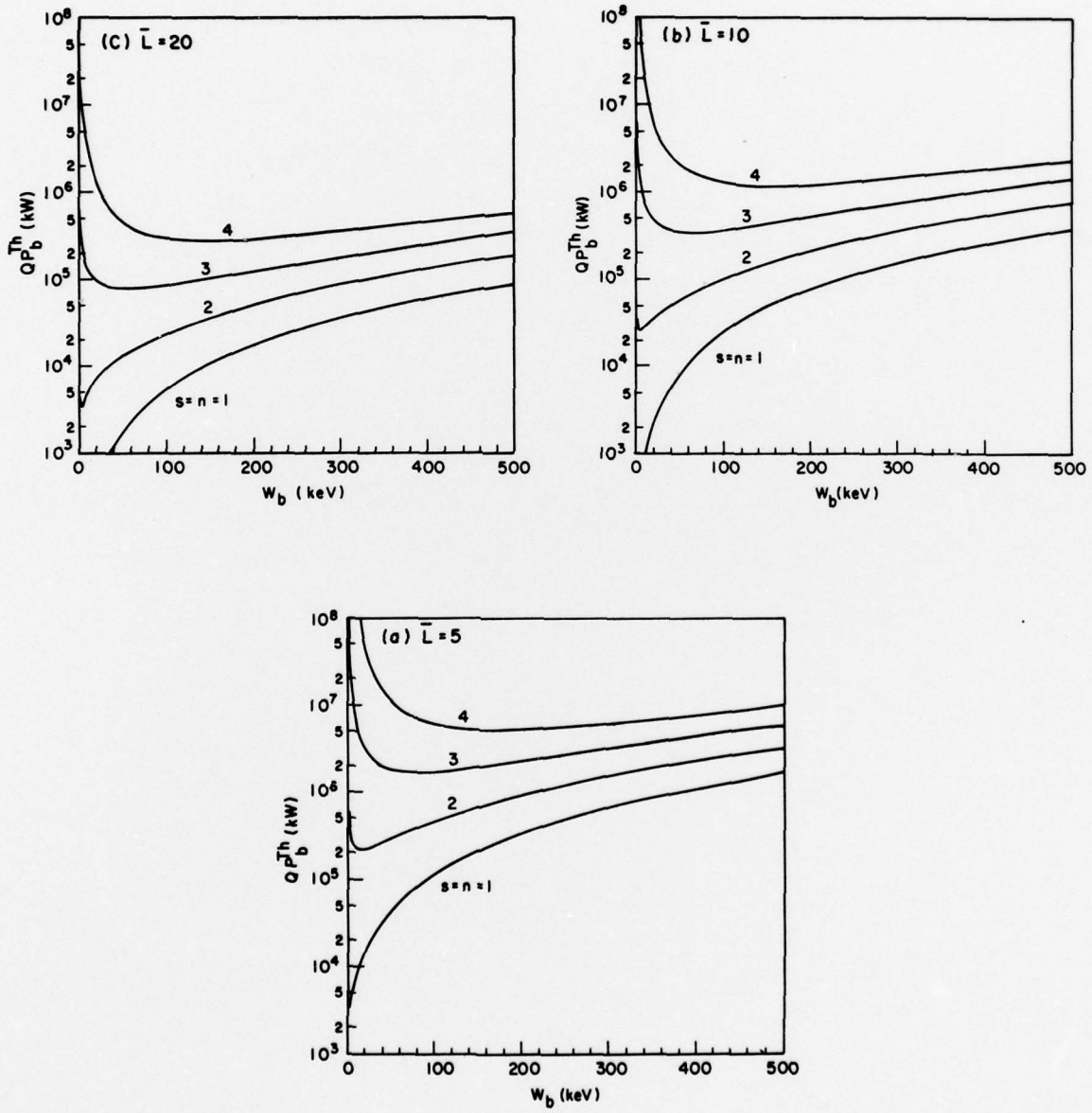


Fig. 7 – Threshold beam power ($P_b^{Th}$) times $Q$ versus beam kinetic energy ($W_b$) for $l = 1$, $n = s$, $v_{\perp 0}/v_{z0} = 1.5$, and (a) $\bar{L} = 5$, (b) $\bar{L} = 10$, (c) $\bar{L} = 20$. The beam guiding center position $\bar{r}_0$ is so chosen that $H_s(x_n\bar{r}_0, x_n\bar{r}_L)$ falls on its first peak with respect to $x_n\bar{r}_0$ (see Fig. 5). The magnetic field $B_0$ has been specified to maximize the beam energy low (see point $X$ on Fig. 6).